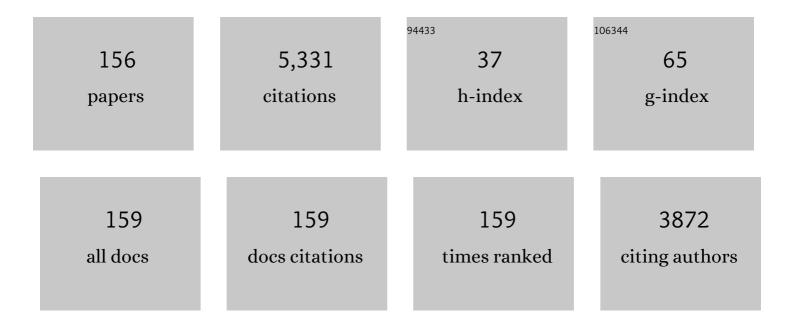
## Ravinder R Regatte

List of Publications by Year in descending order

Source: https://exaly.com/author-pdf/4601476/publications.pdf Version: 2024-02-01



#	Article	IF	CITATIONS
1	Optimization of spinâ€lock times in T <sub>1ï</sub> mapping of knee cartilage: Cramérâ€Rao bounds versus matched samplingâ€fitting. Magnetic Resonance in Medicine, 2022, 87, 1418-1434.	3.0	11
2	Simultaneous bilateral T <sub>1</sub> , T <sub>2</sub> , and T <sub>1ï</sub> relaxation mapping of the hip joint with magnetic resonance fingerprinting. NMR in Biomedicine, 2022, 35, e4651.	2.8	10
3	Injectable recombinant block polymer gel for sustained delivery of therapeutic protein in post traumatic osteoarthritis. Biomaterials, 2022, 281, 121370.	11.4	19
4	Alternating Learning Approach for Variational Networks and Undersampling Pattern in Parallel MRI Applications. IEEE Transactions on Computational Imaging, 2022, 8, 449-461.	4.4	7
5	Performance Comparison of Compressed Sensing Algorithms for Accelerating T <sub>1ï</sub> Mapping of Human Brain. Journal of Magnetic Resonance Imaging, 2021, 53, 1130-1139.	3.4	3
6	Musculoskeletal MR Imaging Applications at Ultra-High (7T) Field Strength. Magnetic Resonance Imaging Clinics of North America, 2021, 29, 117-127.	1.1	3
7	Simultaneous T <sub>1</sub> , T <sub>2</sub> , and T <sub>1ï</sub> relaxation mapping of the lower leg muscle with MR fingerprinting. Magnetic Resonance in Medicine, 2021, 86, 372-381.	3.0	14
8	Measurement of <scp>Threeâ€Dimensional</scp> Internal Dynamic Strains in the Intervertebral Disc of the Lumbar Spine With Mechanical Loading and Goldenâ€Angle Radial Sparse Parallelâ€Magnetic Resonance Imaging. Journal of Magnetic Resonance Imaging, 2021, 54, 486-496.	3.4	13
9	Dynamic 31P-MRI and 31P-MRS of lower leg muscles in heart failure patients. Scientific Reports, 2021, 11, 7412.	3.3	6
10	Pilot study quantifying muscle glycosaminoglycan using bi-exponential T1ï•mapping in patients with muscle stiffness after stroke. Scientific Reports, 2021, 11, 13951.	3.3	4
11	Lower extremity MRI following 10-week supervised exercise intervention in patients with diabetic peripheral neuropathy. BMJ Open Diabetes Research and Care, 2021, 9, e002312.	2.8	5
12	Fast data-driven learning of parallel MRI sampling patterns for large scale problems. Scientific Reports, 2021, 11, 19312.	3.3	12
13	In vivo tibiofemoral cartilage strain mapping under static mechanical loading using continuous GRASPâ€MRI. Journal of Magnetic Resonance Imaging, 2020, 51, 426-434.	3.4	9
14	Accelerated mono―and biexponential 3D‶1ï•relaxation mapping of knee cartilage using golden angle radial acquisitions and compressed sensing. Magnetic Resonance in Medicine, 2020, 83, 1291-1309.	3.0	14
15	Volumetric multicomponent T <sub>1Ï</sub> relaxation mapping of the human liver under free breathing at 3T. Magnetic Resonance in Medicine, 2020, 83, 2042-2050.	3.0	11
16	Current status of functional MRI of osteoarthritis for diagnosis and prognosis. Current Opinion in Rheumatology, 2020, 32, 102-109.	4.3	12
17	Rapid mono and biexponential 3D-T1ϕmapping of knee cartilage using variational networks. Scientific Reports, 2020, 10, 19144.	3.3	11
18	Fast multicomponent 3D―T 1ϕrelaxometry. NMR in Biomedicine, 2020, 33, e4318.	2.8	5

#	Article	IF	CITATIONS
19	MR fingerprinting for rapid simultaneous T <sub>1</sub> , T <sub>2</sub> , and <i>T</i> <sub>1</sub> <i><sub>i</sub></i> relaxation mapping of the human articular cartilage at 3T. Magnetic Resonance in Medicine, 2020, 84, 2636-2644.	3.0	25
20	T1ï•Mapping for Musculoskeletal Pain Diagnosis: Case Series of Variation of Water Bound Glycosaminoglycans Quantification before and after Fascial Manipulation® in Subjects with Elbow Pain. International Journal of Environmental Research and Public Health, 2020, 17, 708.	2.6	19
21	3T chemical shiftâ€encoded MRI: Detection of altered proximal femur marrow adipose tissue composition in glucocorticoid users and validation with magnetic resonance spectroscopy. Journal of Magnetic Resonance Imaging, 2019, 50, 490-496.	3.4	16
22	Assessment of frequency drift on CEST MRI and dynamic correction: application to gagCEST at 7 T. Magnetic Resonance in Medicine, 2019, 81, 573-582.	3.0	35
23	3T chemical shift-encoded MRI: Detection of altered proximal femur marrow adipose tissue composition in glucocorticoid users and validation with magnetic resonance spectroscopy. Journal of Magnetic Resonance Imaging, 2019, 50, spcone-spcone.	3.4	10
24	Quantifying muscle glycosaminoglycan levels in patients with post-stroke muscle stiffness using T1Ï• MRI. Scientific Reports, 2019, 9, 14513.	3.3	16
25	The discrete Fourier transform for golden angle linogram sampling. Inverse Problems, 2019, 35, 125004.	2.0	1
26	3Dâ€T <sub>1Ï</sub> prepared zero echo timeâ€based PETRA sequence for in vivo biexponential relaxation mapping of semisolid shortâ€T <sub>2</sub> tissues at 3 T. Journal of Magnetic Resonance Imaging, 2019, 50, 1207-1218.	3.4	8
27	Monotone FISTA With Variable Acceleration for Compressed Sensing Magnetic Resonance Imaging. IEEE Transactions on Computational Imaging, 2019, 5, 109-119.	4.4	24
28	Biexponential T <sub>1Ï</sub> relaxation mapping of human knee menisci. Journal of Magnetic Resonance Imaging, 2019, 50, 824-835.	3.4	5
29	MRI of synovitis and joint fluid. Journal of Magnetic Resonance Imaging, 2019, 49, 1512-1527.	3.4	28
30	Compressed sensing acceleration of biexponential 3Dâ€T <sub>1Ï</sub> relaxation mapping of knee cartilage. Magnetic Resonance in Medicine, 2019, 81, 863-880.	3.0	20
31	3-T MR Imaging of Proximal Femur Microarchitecture in Subjects with and without Fragility Fracture and Nonosteoporotic Proximal Femur Bone Mineral Density. Radiology, 2018, 287, 608-619.	7.3	21
32	Accelerating 3Dâ€T <sub>1Ï</sub> mapping of cartilage using compressed sensing with different sparse and low rank models. Magnetic Resonance in Medicine, 2018, 80, 1475-1491.	3.0	40
33	Bi-exponential 3D-T1ϕmapping of whole brain at 3 T. Scientific Reports, 2018, 8, 1176.	3.3	20
34	Quadrupolar jumpâ€andâ€return pulse sequence for fluidâ€suppressed sodium MRI of the knee joint at 7T. Magnetic Resonance in Medicine, 2018, 80, 641-647.	3.0	3
35	Biexponential T <sub>2</sub> relaxation estimation of human knee cartilage in vivo at 3T. Journal of Magnetic Resonance Imaging, 2018, 47, 809-819.	3.4	18
36	Longitudinal study of sodium MRI of articular cartilage in patients with knee osteoarthritis: initial experience with 16-month follow-up. European Radiology, 2018, 28, 133-142.	4.5	21

#	Article	IF	CITATIONS
37	Subchondral bone microarchitecture analysis in the proximal tibia at 7-T MRI. Acta Radiologica, 2018, 59, 716-722.	1.1	3
38	Rapid compositional mapping of knee cartilage with compressed sensing MRI. Journal of Magnetic Resonance Imaging, 2018, 48, 1185-1198.	3.4	21
39	MR Imaging of the Musculoskeletal System Using Ultrahigh Field (7T) MR Imaging. PET Clinics, 2018, 13, 551-565.	3.0	3
40	Chemical shift-encoded MRI for assessment of bone marrow adipose tissue fat composition: Pilot study in premenopausal versus postmenopausal women. Magnetic Resonance Imaging, 2018, 53, 148-155.	1.8	29
41	Isotropic morphometry and multicomponent T <sub>1</sub> ï•mapping of human knee articular cartilage in vivo at 3T. Journal of Magnetic Resonance Imaging, 2018, 48, 1707-1716.	3.4	10
42	The Emerging Role of 7 Tesla MRI in Musculoskeletal Imaging. Current Radiology Reports, 2018, 6, 1.	1.4	1
43	Serum Urate Levels Predict Joint Space Narrowing in Nonâ€Gout Patients With Medial Knee Osteoarthritis. Arthritis and Rheumatology, 2017, 69, 1213-1220.	5.6	40
44	MRI assessment of bone structure and microarchitecture. Journal of Magnetic Resonance Imaging, 2017, 46, 323-337.	3.4	86
45	A low-cost Mr compatible ergometer to assess post-exercise phosphocreatine recovery kinetics. Magnetic Resonance Materials in Physics, Biology, and Medicine, 2017, 30, 281-289.	2.0	5
46	Magnetization transfer in a partly deuterated lyotropic liquid crystal by single- and dual-frequency RF irradiations. Journal of Magnetic Resonance, 2017, 281, 141-150.	2.1	2
47	Juvenile Particulate Osteochondral Allograft for Treatment of Osteochondral Lesions of the Talus: Detection of Altered Repair Tissue Biochemical Composition Using 7 Tesla MRI and T2 Mapping. Journal of Foot and Ankle Surgery, 2017, 56, 26-29.	1.0	6
48	Bi-component T1ï•and T2 Relaxation Mapping of Skeletal Muscle In-Vivo. Scientific Reports, 2017, 7, 14115.	3.3	26
49	Biexponential <i>T</i> <sub>1ï</sub> relaxation mapping of human knee cartilage <i>in vivo</i> at 3ÂT. NMR in Biomedicine, 2017, 30, e3760.	2.8	41
50	7T MRI of distal radius trabecular bone microarchitecture: How trabecular bone quality varies depending on distance from endâ€ofâ€bone. Journal of Magnetic Resonance Imaging, 2017, 45, 872-878.	3.4	5
51	Chapter 7 Uniform-MT Method to Separate CEST Contrast from MT Effects. , 2017, , 97-120.		Ο
52	Chapter 16 Cartilage and Intervertebral Disc Imaging and Glycosaminoglycan Chemical Exchange Saturation Transfer (gagCEST) Experiment. , 2017, , 377-398.		0
53	A flexible nested sodium and proton coil array with wideband matching for knee cartilage MRI at 3T. Magnetic Resonance in Medicine, 2016, 76, 1325-1334.	3.0	27
54	Trabecular bone characterization on the continuum of plates and rods using <i>in vivo</i> MR imaging and volumetric topological analysis. Physics in Medicine and Biology, 2016, 61, N478-N496.	3.0	10

#	Article	IF	CITATIONS
55	Relationship between meniscal integrity and risk factors for cartilage degeneration. Knee, 2016, 23, 686-691.	1.6	9
56	<i>In vitro</i> study of endogenous CEST agents at 3 T and 7 T. Contrast Media and Molecular Imaging, 2016, 11, 4-14.	0.8	37
57	Bloch equations for proton exchange reactions in an aqueous solution. Concepts in Magnetic Resonance Part A: Bridging Education and Research, 2016, 45A, .	0.5	6
58	Advances in sodium MRI: biomedical applications from head to foot. NMR in Biomedicine, 2016, 29, 94-95.	2.8	2
59	Sodium inversion recovery MRI on the knee joint at 7 T with an optimal control pulse. Journal of Magnetic Resonance, 2016, 262, 33-41.	2.1	8
60	MRI of the Musculoskeletal System: Advanced Applications using High and Ultrahigh Field MRI. Seminars in Musculoskeletal Radiology, 2015, 19, 363-374.	0.7	24
61	3 Tesla MRI detects deterioration in proximal femur microarchitecture and strength in longâ€ŧerm glucocorticoid users compared with controls. Journal of Magnetic Resonance Imaging, 2015, 42, 1489-1496.	3.4	21
62	In vivo measurement reproducibility of femoral neck microarchitectural parameters derived from 3T MR images. Journal of Magnetic Resonance Imaging, 2015, 42, 1339-1345.	3.4	12
63	Classification of sodium MRI data of cartilage using machine learning. Magnetic Resonance in Medicine, 2015, 74, 1435-1448.	3.0	30
64	Feasibility of mapping unidirectional Piâ€ŧoâ€ATP fluxes in muscles of the lower leg at 7.0 Tesla. Magnetic Resonance in Medicine, 2015, 74, 225-230.	3.0	5
65	Measurement reproducibility of magnetic resonance imaging-based finite element analysis of proximal femur microarchitecture for in vivo assessment of bone strength. Magnetic Resonance Materials in Physics, Biology, and Medicine, 2015, 28, 407-412.	2.0	15
66	Transfer Rate Edited experiment for the selective detection of Chemical Exchange via Saturation Transfer (TRE-CEST). Journal of Magnetic Resonance, 2015, 256, 43-51.	2.1	14
67	7T MRI detects deterioration in subchondral bone microarchitecture in subjects with mild knee osteoarthritis as compared with healthy controls. Journal of Magnetic Resonance Imaging, 2015, 41, 1311-1317.	3.4	20
68	Investigation of Regional Influence of Magic-Angle Effect on T2 in Human Articular Cartilage with Osteoarthritis at 3 T. Academic Radiology, 2015, 22, 87-92.	2.5	20
69	T1rho MRI at 3T of menisci in patients with acute anterior cruciate ligament (ACL) injury. Journal of Magnetic Resonance Imaging, 2015, 41, 544-549.	3.4	16
70	T <sub>1Ï</sub> MRI of human musculoskeletal system. Journal of Magnetic Resonance Imaging, 2015, 41, 586-600.	3.4	80
71	7ÂTesla MRI of bone microarchitecture discriminates between women without and with fragility fractures who do not differ by bone mineral density. Journal of Bone and Mineral Metabolism, 2015, 33, 285-293.	2.7	34
72	Repeatability of Quantitative Sodium Magnetic Resonance Imaging for Estimating Pseudo-Intracellular Sodium Concentration and Pseudo-Extracellular Volume Fraction in Brain at 3 T. PLoS ONE, 2015, 10, e0118692.	2.5	26

#	Article	IF	CITATIONS
73	Why Buy an Expensive (\$7 Million) 7T MRI System for Biomedical Research?. Journal of Magnetic Resonance Imaging, 2014, 40, 280-282.	3.4	2
74	Finite Element Analysis Applied to 3-T MR Imaging of Proximal Femur Microarchitecture: Lower Bone Strength in Patients with Fragility Fractures Compared with Control Subjects. Radiology, 2014, 272, 464-474.	7.3	72
75	MRI of the hip at 7T: Feasibility of bone microarchitecture, high-resolution cartilage, and clinical imaging. Journal of Magnetic Resonance Imaging, 2014, 39, 1384-1393.	3.4	36
76	Feasibility of threeâ€dimensional MRI of proximal femur microarchitecture at 3 tesla using 26 receive elements without and with parallel imaging. Journal of Magnetic Resonance Imaging, 2014, 40, 229-238.	3.4	30
77	T1rho MRI of menisci in patients with osteoarthritis at 3 Tesla: A preliminary study. Journal of Magnetic Resonance Imaging, 2014, 40, 588-595.	3.4	16
78	Sodium MRI: Methods and applications. Progress in Nuclear Magnetic Resonance Spectroscopy, 2014, 79, 14-47.	7.5	176
79	Concurrent saturation transfer contrast in in vivo brain by a uniform magnetization transfer MRI. NeuroImage, 2014, 95, 22-28.	4.2	24
80	Quantitative Mapping of Human Cartilage at 3.0T. Academic Radiology, 2014, 21, 463-471.	2.5	44
81	Evaluation of Subchondral Bone Marrow Lipids of Acute Anterior Cruciate Ligament (ACL)-Injured Patients at 3ÂT. Academic Radiology, 2014, 21, 758-766.	2.5	6
82	A method for estimating intracellular sodium concentration and extracellular volume fraction in brain in vivo using sodium magnetic resonance imaging. Scientific Reports, 2014, 4, 4763.	3.3	87
83	Three-dimensional Saturation Transfer 31P-MRI in Muscles of the Lower Leg at 3.0 T. Scientific Reports, 2014, 4, 5219.	3.3	11
84	Advanced MRI of Cartilage and Subchondral Bone in Osteoarthritis. , 2014, , 177-191.		0
85	MAGNETIC RESONANCE IMAGING OF CARTILAGE REPAIR WITH A FOCUS ON SUBCHONDRAL BONE. , 2014, , 305-324.		0
86	SODIUM IMAGING OF THE KNEE JOINT REPAIR. , 2014, , 273-303.		0
87	Spectrally selective 3D TSE imaging of phosphocreatine in the human calf muscle at 3 T. Magnetic Resonance in Medicine, 2013, 69, 812-817.	3.0	19
88	Optimal gadolinium concentration for direct MR arthrography at high field strength up to 7T: In vitro model. Egyptian Journal of Radiology and Nuclear Medicine, 2013, 44, 283-289.	0.6	0
89	High resolution morphologic imaging and T2 mapping of cartilage at 7ÂTesla: comparison of cartilage repair patients and healthy controls. Magnetic Resonance Materials in Physics, Biology, and Medicine, 2013, 26, 539-548.	2.0	19
90	Uniform magnetization transfer in chemical exchange saturation transfer magnetic resonance imaging. Scientific Reports, 2013, 3, 1707.	3.3	27

#	Article	IF	CITATIONS
91	Relationship between knee alignment and T1ϕvalues of articular cartilage and menisci in patients with knee osteoarthritis. European Journal of Radiology, 2013, 82, 1946-1952.	2.6	16
92	Design of a nested eightâ€channel sodium and fourâ€channel proton coil for 7T knee imaging. Magnetic Resonance in Medicine, 2013, 70, 259-268.	3.0	51
93	Articular Cartilage: Evaluation with Fluid-suppressed 7.0-T Sodium MR Imaging in Subjects with and Subjects without Osteoarthritis. Radiology, 2013, 268, 481-491.	7.3	78
94	Threeâ€dimensional mapping of the creatine kinase enzyme reaction rate in muscles of the lower leg. NMR in Biomedicine, 2013, 26, 1142-1151.	2.8	24
95	Dynamic threeâ€dimensional imaging of phosphocreatine recovery kinetics in the human lower leg muscles at 3T and 7T: a preliminary study. NMR in Biomedicine, 2013, 26, 348-356.	2.8	46
96	Biomedical applications of sodium MRI in vivo. Journal of Magnetic Resonance Imaging, 2013, 38, 511-529.	3.4	198
97	3Dâ€mapping of phosphocreatine concentration in the human calf muscle at 7 T: Comparison to 3 T. Magnetic Resonance in Medicine, 2013, 70, 1619-1625.	3.0	25
98	Simultaneous Visualization of Nerves and Vessels of the Lower Extremities Using Magnetization-Prepared Susceptibility Weighted Magnetic Resonance Imaging at 3.0 T. Operative Neurosurgery, 2012, 70, ons1-ons7.	0.8	3
99	Rapid 3Dâ€imaging of phosphocreatine recovery kinetics in the human lower leg muscles with compressed sensing. Magnetic Resonance in Medicine, 2012, 68, 1738-1746.	3.0	28
100	T1rho MRI of menisci and cartilage in patients with osteoarthritis at 3T. European Journal of Radiology, 2012, 81, 2329-2336.	2.6	73
101	Relation between cartilage volume and meniscal contact in medial osteoarthritis of the knee. Knee, 2012, 19, 896-901.	1.6	20
102	Reproducibility and repeatability of quantitative sodium magnetic resonance imaging in vivo in articular cartilage at 3 T and 7 T. Magnetic Resonance in Medicine, 2012, 68, 841-849.	3.0	52
103	Improved assessment of cartilage repair tissue using fluid-suppressed 23Na inversion recovery MRI at 7 Tesla: preliminary results. European Radiology, 2012, 22, 1341-1349.	4.5	41
104	Anterior–posterior stability of the knee by an MR image subtraction method. Knee, 2012, 19, 445-449.	1.6	9
105	Compressed sensing sodium MRI of cartilage at 7T: Preliminary study. Journal of Magnetic Resonance, 2012, 214, 360-365.	2.1	85
106	Isolating chemical exchange saturation transfer contrast from magnetization transfer asymmetry under two-frequency rf irradiation. Journal of Magnetic Resonance, 2012, 215, 56-63.	2.1	71
107	Assessment of glycosaminoglycan concentration changes in the intervertebral disc via chemical exchange saturation transfer. NMR in Biomedicine, 2012, 25, 255-261.	2.8	70
108	Sodium relaxation times in the knee joint <i>in vivo</i> at 7T. NMR in Biomedicine, 2012, 25, 530-537.	2.8	52

#	Article	IF	CITATIONS
109	Assessment of subchondral bone marrow lipids in healthy controls and mild osteoarthritis patients at 3T. NMR in Biomedicine, 2012, 25, 545-555.	2.8	12
110	Comparison of a 28â€channel receive array coil and quadrature volume coil for morphologic imaging and T2 mapping of knee cartilage at 7T. Journal of Magnetic Resonance Imaging, 2012, 35, 441-448.	3.4	35
111	In vivo estimation of bone stiffness at the distal femur and proximal tibia using ultra-high-field 7-Tesla magnetic resonance imaging and micro-finite element analysis. Journal of Bone and Mineral Metabolism, 2012, 30, 243-251.	2.7	24
112	MR Imaging Assessment of Articular Cartilage Repair Procedures. Magnetic Resonance Imaging Clinics of North America, 2011, 19, 323-337.	1.1	19
113	Sodium MRI with fluid suppression: will it improve early detection of osteoarthritis?. Imaging in Medicine, 2011, 3, 1-4.	0.0	6
114	Uniform saturation of a strongly coupled spin system by two-frequency irradiation. Journal of Chemical Physics, 2011, 134, 234504.	3.0	29
115	Reproducibility of subregional trabecular bone micro-architectural measures derived from 7-Tesla magnetic resonance images. Magnetic Resonance Materials in Physics, Biology, and Medicine, 2011, 24, 121-125.	2.0	15
116	Quantitative assessment of trabecular bone micro-architecture of the wrist via 7ÂTesla MRI: preliminary results. Magnetic Resonance Materials in Physics, Biology, and Medicine, 2011, 24, 191-199.	2.0	10
117	Quantitative magnetic resonance imaging evidence of synovial proliferation is associated with radiographic severity of knee osteoarthritis. Arthritis and Rheumatism, 2011, 63, 2983-2991.	6.7	114
118	The Fate of Oral Glucosamine Traced by <sup>13</sup> C Labeling in the Dog. Cartilage, 2011, 2, 279-285.	2.7	4
119	Does joint alignment affect the T2 values of cartilage in patients with knee osteoarthritis?. European Radiology, 2010, 20, 1532-1538.	4.5	28
120	3D 23Na MRI of human skeletal muscle at 7ÂTesla: initial experience. European Radiology, 2010, 20, 2039-2046.	4.5	43
121	Sodium inversion recovery MRI of the knee joint in vivo at 7T. Journal of Magnetic Resonance, 2010, 207, 42-52.	2.1	68
122	MRI of the wrist at 7 tesla using an eight hannel array coil combined with parallel imaging: Preliminary results. Journal of Magnetic Resonance Imaging, 2010, 31, 740-746.	3.4	54
123	Optimal control NMR differentiation between fast and slow sodium. Chemical Physics Letters, 2010, 494, 331-336.	2.6	14
124	Biochemical and Physiological MR Imaging of Skeletal Muscle at 7 Tesla and Above. Seminars in Musculoskeletal Radiology, 2010, 14, 269-278.	0.7	14
125	T2 Measurements of Cartilage in Osteoarthritis Patients With Meniscal Tears. American Journal of Roentgenology, 2009, 193, W411-W415.	2.2	42
126	In Vivo 7.0-Tesla Magnetic Resonance Imaging of the Wrist and Hand: Technical Aspects and Applications. Seminars in Musculoskeletal Radiology, 2009, 13, 074-084.	0.7	31

#	Article	IF	CITATIONS
127	Optimal excitation of N23a nuclear spins in the presence of residual quadrupolar coupling and quadrupolar relaxation. Journal of Chemical Physics, 2009, 131, 174501.	3.0	17
128	Relaxation times of skeletal muscle metabolites at 7T. Journal of Magnetic Resonance Imaging, 2009, 29, 1457-1464.	3.4	38
129	Rapid isotropic 3Dâ€ <b>s</b> odium MRI of the knee joint in vivo at 7T. Journal of Magnetic Resonance Imaging, 2009, 30, 606-614.	3.4	91
130	Selective detection of ordered sodium signals by a jump-and-return pulse sequence. Journal of Magnetic Resonance, 2009, 200, 126-129.	2.1	12
131	MRI Analysis of Anteroposterior Stability in the Normal Human Knee. , 2009, , .		Ο
132	Rapid 3Dâ€T <sub>1</sub> mapping of cartilage with variable flip angle and parallel imaging at 3.0T. Journal of Magnetic Resonance Imaging, 2008, 27, 154-161.	3.4	28
133	Adaptations in trabecular bone microarchitecture in Olympic athletes determined by 7T MRI. Journal of Magnetic Resonance Imaging, 2008, 27, 1089-1095.	3.4	65
134	Characterization of bovine patellar cartilage by NMR. NMR in Biomedicine, 2008, 21, 289-295.	2.8	39
135	Clean demarcation of cartilage tissue 23Na by inversion recovery. Journal of Magnetic Resonance, 2008, 193, 207-209.	2.1	32
136	Novel Contrast Mechanisms at 3 Tesla and 7 Tesla. Seminars in Musculoskeletal Radiology, 2008, 12, 266-280.	0.7	26
137	Assessment of glycosaminoglycan concentration <i>in vivo</i> by chemical exchange-dependent saturation transfer (gagCEST). Proceedings of the National Academy of Sciences of the United States of America, 2008, 105, 2266-2270.	7.1	511
138	Optimal nuclear magnetic resonance excitation schemes for the central transition of a spin 3/2 in the presence of residual quadrupolar coupling. Journal of Chemical Physics, 2008, 129, 224510.	3.0	16
139	Ultra-high-field MRI of the musculoskeletal system at 7.0T. Journal of Magnetic Resonance Imaging, 2007, 25, 262-269.	3.4	136
140	Three-dimensional spin-lock magnetic resonance imaging of the shoulder joint at 3 T: initial experience. Skeletal Radiology, 2007, 36, 1171-1175.	2.0	6
141	Magic sandwich echo relaxation mapping of anisotropic systems. Magnetic Resonance Imaging, 2007, 25, 433-438.	1.8	6
142	Ultra–High-Field MRI of Knee Joint at 7.0T: Preliminary Experience. Academic Radiology, 2006, 13, 1135-1142.	2.5	44
143	Rapid 3D-T1ï•mapping of the knee joint at 3.0T with parallel imaging. Magnetic Resonance in Medicine, 2006, 56, 563-571.	3.0	60
144	Behavior of ordered sodium in enzymatically depleted cartilage tissue. Magnetic Resonance in Medicine, 2006, 56, 1151-1155.	3.0	28

#	Article	IF	CITATIONS
145	T1ϕrelaxation mapping in human osteoarthritis (OA) cartilage: Comparison of T1ϕwith T2. Journal of Magnetic Resonance Imaging, 2006, 23, 547-553.	3.4	296
146	3D-T1ï•quantitation of patellar cartilage at 3.0T. Journal of Magnetic Resonance Imaging, 2006, 24, 1357-1363.	3.4	27
147	Depth-dependent proton magnetization transfer in articular cartilage. Journal of Magnetic Resonance Imaging, 2005, 22, 318-323.	3.4	25
148	Proteoglycan Loss in Human Knee Cartilage: Quantitation with Sodium MR Imaging—Feasibility Study. Radiology, 2004, 231, 900-905.	7.3	168
149	In vivo measurement of T1? dispersion in the human brain at 1.5 tesla. Journal of Magnetic Resonance Imaging, 2004, 19, 403-409.	3.4	60
150	Reduction of residual dipolar interaction in cartilage by spin-lock technique. Magnetic Resonance in Medicine, 2004, 52, 1103-1109.	3.0	126
151	In vivo quantification ofT1? using a multislice spin-lock pulse sequence. Magnetic Resonance in Medicine, 2004, 52, 1453-1458.	3.0	51
152	Proton MRI of metabolically produced H217O using an efficient 17O2 delivery system. NeuroImage, 2004, 22, 611-618.	4.2	29
153	Three-dimensional T1?-weighted MRI at 1.5 Tesla. Journal of Magnetic Resonance Imaging, 2003, 17, 730-736.	3.4	59
154	Indirect17O-magnetic resonance imaging of cerebral blood flow in the rat. Magnetic Resonance in Medicine, 2003, 49, 479-487.	3.0	34
155	T1ϕMR Imaging of the Human Wrist in Vivo. Academic Radiology, 2003, 10, 614-619.	2.5	27
156	Probing Rat Brain Oxygenation with Near-Infrared Spectroscopy (NIRS) and Magnetic Resonance Imaging (MRI). Advances in Experimental Medicine and Biology, 2003, 510, 199-204.	1.6	8